Journal of Electroanalytical Chemistry 624 (2008) 14–20

Contents lists available at ScienceDirect

Journal of Electroanalytical Chemistry

journal homepage: www.elsevier.com/locate/jelechem

Constant phase elements, depressed arcs and analytic continuation: A critique

Bosco Emmanuel *, Modeling and Simulation Group

Central Electrochemical Research Institute, Karaikudi, India

ARTICLE INFO

Article history:
Received 5 June 2008
Accepted 12 July 2008
Available online 22 July 2008

Keywords:
AC impedance
Constant phase elements
Depressed arcs
Analytic continuation
Nyquist plots
Bode phase plots

ABSTRACT

The connection between the constant phase element (CPE) and the depressed arcs often observed in the Nyquist plane is critically analyzed using the analytic continuation principle enunciated earlier by the author. A major inconsistency is pointed out in a model presently used to explain these depressed arcs. A new model is advanced which removes this inconsistency and also has a clear physical basis. A set of exact analytic results are reported which may be used as diagnostic criteria for testing experimental impedance data against different models. Several Nyquist and Bode phase plots are presented as illustrations. Experimental systems where the proposed model will be a good candidate are also discussed.

1. Introduction

In two earlier papers by the author [1,2], analytic continuation was used to connect the ac response of arbitrary electrode geometries to the corresponding secondary current distributions. Several Hull cell geometries, the rectangular pore, the saw-tooth and a fractal geometry were studied and the method was shown to provide a bench-mark for evaluating the reliability of approximate theories such as the Transmission Line Model [3–5]. In this paper we take up the problem of depressed arcs often observed in the Nyquist plane for rough electrodes where a Faradaic reaction takes place in addition to capacitive charging. [In this paper, the term "rough" will apply to any electrode whose purely capacitive behavior follows a CPE power law.] A major inconsistency is pointed out in a model used to explain these depressed arcs and a new model is proposed which removes this inconsistency. Section 2 summarizes the prior developments and in Section 3 we formulate the method of analytic continuation in a convenient dimensionless form by introducing a length scale in the problem and further show how any candidate model should satisfy a consistency condition in view of the fundamental equations which govern the ac response. We advance, in Section 4, a model which satisfies this consistency condition and is also able to reproduce the depressed Nyquist arcs. Section 5 reports a set of exact analytic results which may be used as diagnostic criteria for this new model and tabulate it along with the criteria for the old models facilitating the comparison of models among themselves and with the experimental data. Discussion, Summary and Conclusions are placed in the last section.

2. Prior developments

For perfectly polarisable solid electrodes (i.e. with purely capacitive charging), the impedance response is often represented by the so-called constant phase element (CPE):

$$Z = \frac{A}{(j\omega)^{\alpha}}. \tag{1}$$

Different researchers have tried to explain the CPE differently, invoking for example a distribution of relaxation time constants, rough/fractal electrode geometries, pore structures and non-uniform current–potential distributions. Though the theory of CPE is not yet a completely settled issue, experiments have established, beyond reasonable doubt, Eq. (1) for a large number of experimental systems.

Eq. (1) does not include Faradaic reactions. Once we bring in a redox activity at the interface, the inclined CPE-line in the Nyquist plane changes into a depressed arc. Some workers [6,7] have tried to explain these arcs by incorporating an over-all resistance R in parallel with the CPE in Eq. (1) and curve-fit these arcs with an equation of the form:

$$Z = \frac{1}{\frac{1}{R} + \frac{(j\omega)^{\alpha}}{A}}. \tag{2}$$

Others have used a different form:

$$Z = \frac{1}{B}\left(\frac{1}{\frac{1}{R} + j\omega C}\right)^{\alpha}. \tag{3}$$

It is important to note the differences in the functional forms in Eqs. (2) and (3): Both the Faradaic and non-Faradaic parts are subjected

* Tel.: +91 4565 228986; fax: +91 4565 227779.
E-mail address: boscoemmanuel@yahoo.co.in.

0022-0728/$ - see front matter
doi:10.1016/j.jelechem.2008.07.014

Nomenclature

Z, Y	impedance and admittance	ϕ_0	amplitude of the ac signal
ω	frequency	ℓ	length scale
$\alpha, \alpha_A, \alpha_B$	CPE exponents	Wa^*	complex Wagner number
R, R_{ct}	charge-transfer resistances	κ	conductivity of the electrolyte
$C, C_{dl,A}, C_{dl,B}$	double-layer capacities	A, A_A, A_B	effective areas of different regions
ϕ	dimensional or non-dimensional potential		

to the dispersion in Eq. (3), while only the non-Faradaic part is subjected to dispersion in Eq. (2). Further, only Eq. (2) leads to depressed semi-circles and Eq. (3) produces only the Cole-Davidson-type Nyquist response resembling one-fourth of a lemniscate. In an attempt to generalize the CPE to include charge-transfer, diffusion and chemical reactions, de Levie [8] started off from Eq. (3). In a study of hydrogen evolution on lanthanum–phosphate-bonded Ni electrode, Los and co-workers [9] have studied Eq. (2) in addition to Eq. (3) and a 2-CPE model; though its physical basis is not clear, their conclusion is in favor of this 2-CPE model whose experimental fit is slightly better than that of Eq. (3). Hasbach and co-workers [10] used Eq. (3) in combination with the transmission line model to describe the impedance of porous Zn electrodes in weakly alkaline electrolyte.

The models proposed so far to explain the depressed arcs suffer from one or more of the following deficiencies:

(i) A clear physical basis is not provided by the originators of the model.
(ii) The model does not satisfy the consistency condition discussed later on in this paper.
(iii) The model fails to produce the depressed arcs.

For example, the model represented by Eq. (2) suffers from the deficiency (ii) and that involving Eq. (3) has the deficiency (iii). Other models reported in the literature have one or more of these deficiencies.

3. Non-dimensional form of the equations governing the ac response and the consistency condition

In this section, we write the equations which govern the ac response in a convenient non-dimensional form for use in subsequent sections and also deduce the consistency condition referred to in the earlier section.

Following [1,2], we write the governing equations as

$$\nabla^2\phi = 0 \tag{4}$$

with the boundary condition

$$-\kappa\nabla_n\phi = \left(\frac{1}{R_{ct}} + j\omega C_{dl}\right)(\phi_0 - \phi), \tag{5}$$

at the working electrode. The boundary conditions at the counter electrode and at the walls of the cell, which may be taken to have their usual forms, are not important for the present work. The notations, though obvious, are collected together at the end of the article.

We pass to the dimensionless form by dividing the potential ϕ by the amplitude of the ac signal ϕ_0 and the spatial co-ordinates (x, y, z) by a length scale ℓ. However, for notational convenience, we retain the symbol ϕ for the dimensionless potential and the ∇ operator now uses the dimensionless co-ordinates $(x/\ell, y/\ell, z/\ell)$. The dimensionless system is:

$$\nabla^2\phi = 0 \tag{6}$$

with

$$-\nabla_n\phi = \left(\frac{\ell}{\kappa R_{ct}} + \frac{j\omega C_{dl}\ell}{\kappa}\right)(1 - \phi), \tag{7}$$

satisfying at the electrode boundary B.

There is essentially only one model parameter in this system, viz.

$$\left(\frac{\ell}{\kappa R_{ct}} + \frac{j\omega C_{dl}\ell}{\kappa}\right), \tag{8}$$

which may be termed the complex Wagner number, Wa^*. Hence, the dimensionless potential depends only on this complex parameter besides the geometrical details of the electrode surface. Now, the expression for admittance is:

$$Y = -\frac{\kappa}{\ell}\int_B \nabla_n\phi \, dB. \tag{9}$$

where ϕ and ∇ are dimensionless and the integral, over the electrode boundary B, has the dimensions of area.

Eq. (9) may be written as

$$Y = \frac{\kappa}{\ell} f(Wa^*). \tag{10}$$

When $R_{ct} = \infty$, for a purely capacitive electrode,

$$Y = \frac{\kappa}{\ell} f(j\omega C_{dl}\ell/\kappa). \tag{11}$$

Comparing this with the experimentally observed CPE response (for perfectly polarisable electrodes)

$$Y = (j\omega)^\alpha/A. \tag{12}$$

We deduce that

$$f(j\omega C_{dl}\ell/\kappa) = (j\omega C_{dl}\ell/\kappa)^\alpha A, \tag{13}$$

where A is a non-trivial area-factor. When $\alpha = 1$, we of course obtain the admittance of the flat electrode

$$Y = j\omega C_{dl}A. \tag{14}$$

where A is now the area of the flat electrode.

Note that, as we are considering only the working electrode impedance, the solution resistance and any counter electrode impedance do not come into the picture, though these may be easily included as was shown in my earlier paper [1].

Now we switch on a charge transfer reaction with a finite R_{ct} on the same working electrode. Analytic continuation leads to the following expression for the admittance:

$$Y = \frac{\kappa}{\ell}\left(\frac{\ell}{\kappa R_{ct}} + \frac{j\omega C_{dl}\ell}{\kappa}\right)^\alpha A. \tag{15}$$

The Nyquist plot corresponding to this admittance is shown in Fig. 1. This is a Cole-Davidson-type impedance and not a depressed semi-circle!

Our conclusion is: The CPE power law in the purely capacitive region is not a sufficient condition for the system to exhibit a depressed semi-circle when a charge transfer reaction is included.

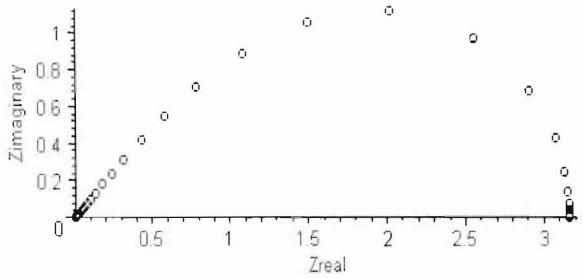

Fig. 1. A plot of Eq. (15) illustrating the Cole-Davidson-type behavior. $R_{ct} = 2500\ \Omega\,cm^2$, $\kappa = 0.1\ S\,cm^{-1}$, $C_{dl} = 20\ \mu F\,cm^{-2}$, and $\alpha = 0.5$.

Once we view the ac response as the analytic continuation of the dc response, we have a simple and powerful method of going back and forth not only between the ac and dc problems but also between the purely capacitive problem and the problem which includes charge transfer. This perspective further provides a consistency condition which any impedance model should satisfy. For example, Eqs. (4) and (5) dictate that the charge-transfer resistance R_{ct} and the double-layer capacitance C_{dl} can appear, in any impedance expression, only in the strict combination:

$$\left(\frac{1}{R_{ct}} + j\omega C_{dl}\right) \tag{16}$$

and not separately. In other words, the impedance can only be a function of

$$\left(\frac{1}{R_{ct}} + j\omega C_{dl}\right)$$

and not of R_{ct} and C_{dl} separately.

Before we close this section, a remark is in order. Though electrochemical impedance spectroscopy (EIS) and the concept of equivalent circuits in Electrochemistry were originally inspired by circuits in Electrical Engineering, an important difference between the two disciplines must be kept in mind by the practitioners of EIS. While electrical engineers have the freedom to assemble and connect the circuit elements in any way they want, electrochemists are constrained by the fundamental governing equations such as (4) and (5). Given the vast collection of circuits which are being employed by electrochemists to-day to curve-fit experimental data in EIS, such constraints and self-consistency conditions should be welcome for they will help to regulate and check the proposed impedance models.

4. A consistent model for the Nyquist arcs

Though Eq. (15) is fundamentally sound, it fails to produce the depressed arcs. In sharp contrast, Eq. (2) produces these arcs; however it does not satisfy the condition enunciated in Section 3. In the present section, we advance a model which has a clear physical basis, satisfies the consistency condition and produces the depressed arcs.

We consider a model for an electrode surface which is electrochemically heterogeneous in the sense that there are two types of regions A and B, with only non-Faradaic processes taking place on A and both Faradaic and non-Faradaic processes on B. Both the regions are in general "rough" in the sense in which it was defined in the beginning of this article. The A-type regions may be realized in actual systems in several ways: depending on the nature of the reacting species and the electrolyte, the A-type region may consist of oxide-covered patches on metal electrodes, specifically adsorbed molecules and ions (e.g. surfactants), surface defect regions energetically unfavorable to charge-transfer or any other agent which poison and deactivate parts of the electrode against charge-transfer (inhibitors in corrosion and painted surfaces with holidays, for example). For this model, the impedance is given by

$$Z = \frac{1}{Y_A + Y_B}, \tag{17}$$

where

$$Y_A = \frac{\kappa}{\ell}\left(\frac{j\omega C_{dl,A}\ell}{\kappa}\right)^{\alpha_A} A_A \tag{18}$$

and

$$Y_B = \frac{\kappa}{\ell}\left(\frac{\ell}{\kappa R_{ct}} + \frac{j\omega C_{dl,B}\ell}{\kappa}\right)^{\alpha_B} A_B. \tag{19}$$

The exponents α_A and α_B can in general be different for A and B type regions and so also their specific capacities $C_{dl,A}$ and $C_{dl,B}$. A_A and A_B are the corresponding effective areas mentioned earlier. While Y_B alone can produce only the Cole-Davidson-type lemniscates in the Nyquist impedance plane, addition of Y_A changes it into depressed arcs which are typical of experimental data. Figs. 2 and 3 show these Nyquist arcs for several settings of α_A, α_B, A_A and A_B. Though the model represented by Eq. (2) (we henceforth call it model I) and that represented by Eqs. (17)–(19) (model II) lead to similar Nyquist arcs, two serious differences between the two must be noted: (i) model I is inconsistent with the fundamental equations, while model II is consistent; (ii) the low and high frequency Nyquist

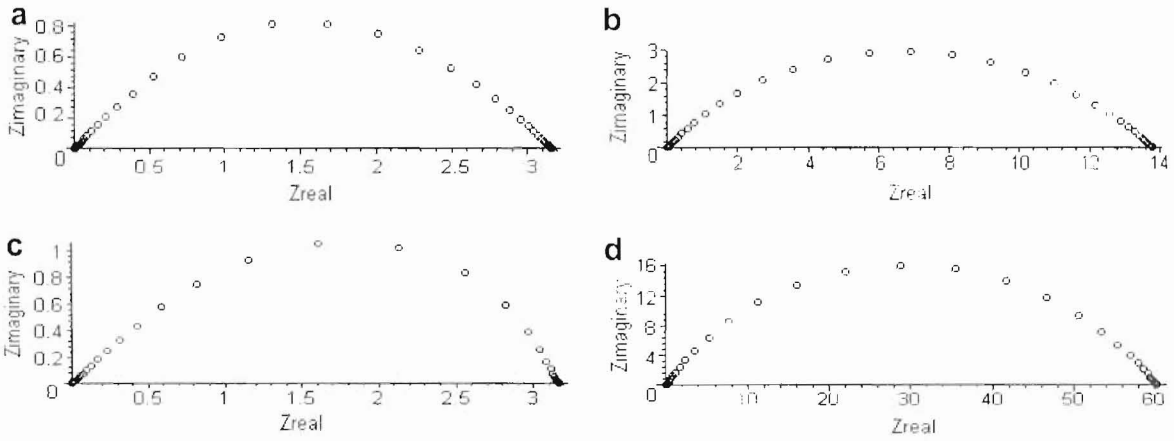

Fig. 2. Plots illustrating the depressed arcs predicted by Eqs. (17)–(19) for model II. (a) $\alpha_A = 0.5$, $\alpha_B = 0.5$, (b) $\alpha_A = 0.5$, $\alpha_B = 0.6$, (c) $\alpha_A = 0.6$, $\alpha_B = 0.5$, and (d) $\alpha_A = 0.6$, $\alpha_B = 0.7$. $C_{dl,A} = C_{dl,B} = 20\ \mu F\,cm^{-2}$. $f_A = 0.5$ and $f_B = 0.5$. f_A and f_B are the effective area fractions of the A- and B-type regions. The values of all other parameters are as in Fig. 1.

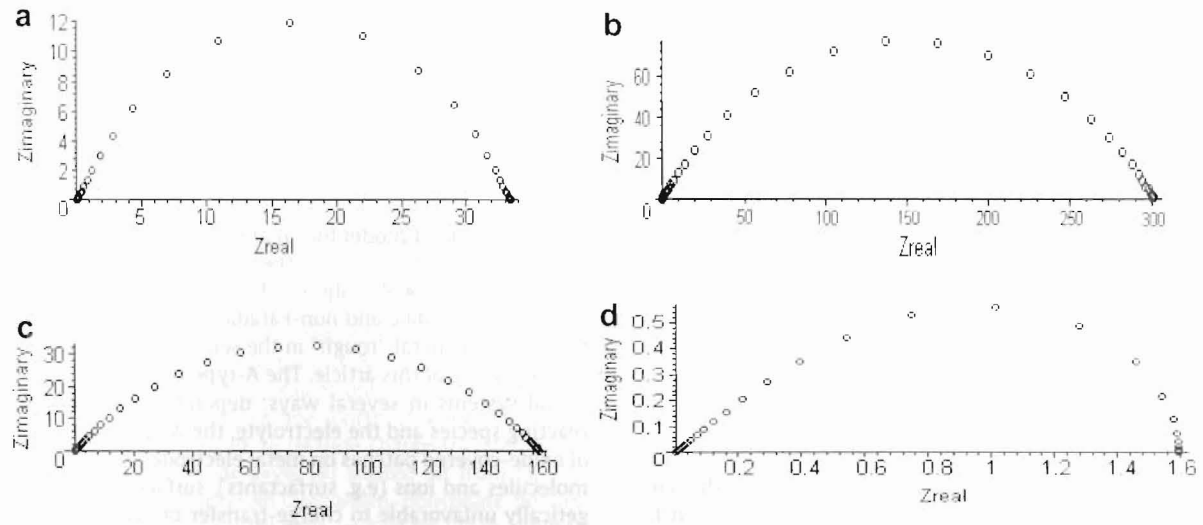

Fig. 3. (a) $\alpha_A = 0.6$, $\alpha_B = 0.7$, $f_A = 0.1$ and $f_B = 0.9$. (b) $\alpha_A = 0.6$, $\alpha_B = 0.7$, $f_A = 0.9$ and $f_B = 0.1$. (c) $\alpha_A = 0.5$, $\alpha_B = 0.5$, $f_A = 0.99$ and $f_B = 0.01$. (d) $\alpha_A = 0.5$, $\alpha_B = 0.5$, $f_A = 0.01$ and $f_B = 0.99$. Other parameters are as in Figs. 1 and 2.

slopes are equal in magnitude(though of course opposite in sign) for model I, while these slopes may in general be different in magnitude for model II depending on the values of α_A and α_B. More about this in the next section. Eq. (15) will be referred to as model III.

We believe that the model represented by Eqs. (17)–(19) is the simplest model which has a clear physical basis, satisfies the consistency condition and produce depressed arcs. There is also a bonus: By varying the model parameters such as α_A, α_B, A_A and A_B, several different Nyquist responses can be realized as special cases: the pure CPE, the lemniscate (or the Cole-Davidson-type) response, the classical semi-circle and the depressed arcs. In this last respect, this model can also serve as a good candidate for curve-fitting experimental impedance data.

5. Diagnostics

We present in this section a set of exact analytic results which can be applied to experimental ac impedance data to validate the different models. Though very often curve-fitting is used to fit experimental impedance data to chosen models, a successful curve-fit cannot be taken to validate a model especially when the model does not have a clear physical basis and mathematical consistency. Hence diagnostic tests are paramount. Before we discuss these diagnostics, let us note that model I will be a special case of model II, if we can set $\alpha_B = 0$ in model II. However, unfortunately for model I, it is well established experimentally that the exponent α ranges only between 0.5 and 1. This is indeed a fortunate situation for our theory enunciated here which rules out model I.

Now we turn to the diagnostics. We have exact analytic results for the three diagnostic properties of the Nyquist response: the low frequency intercept on the real axis, the low and the high frequency slopes. As we mentioned earlier, we have not included the solution resistance in the present treatment and hence the high frequency intercept on the real axis is zero for all the models. These analytic results are listed in Table 1 for the new model along with the corresponding results for the older models, including the Randles circuit, to facilitate a comparison. Except for model II, we have further exact results for the real and imaginary components of the impedance and the frequency corresponding to the maximum point in the Nyquist plot ($Z_{Re,max}$, $Z_{Im,max}$, ω_{max}). The methods by which these analytic results were obtained are sketched in the Appendices. We summarize below the three models (I–III) along with the exact results for the Nyquist maxima ($Z_{Re,max}$, $Z_{Im,max}$, ω_{max}).

Table 1
Diagnostic criteria for some models

Model no.	Intercept on the real axis	Low frequency slope	High frequency slope
I	R	$-\tan(\alpha\pi/2)$	$\tan(\alpha\pi/2)$
II	$\frac{\ell}{\kappa}\left(\frac{\kappa R_{ct}}{\ell}\right)^{\alpha_B} A_B^{-1}$	$-\tan(\alpha_A\pi/2)$	$\tan(\alpha_A\pi/2)$ for $\alpha_A > \alpha_B$ $\tan(\alpha_B\pi/2)$ for $\alpha_B > \alpha_A$
III	$\frac{\ell}{\kappa}\left(\frac{\kappa R_{ct}}{\ell}\right)^{\alpha} A^{-1}$	$-\infty$	$\tan(\alpha\pi/2)$
Classical	R_{ct}	$-\infty$	∞

5.1. Model I

$$Z = \frac{1}{\frac{1}{R} + Y}, \tag{20}$$

where

$$Y = \frac{\kappa}{\ell}\left(\frac{j\omega C_{dl}\ell}{\kappa}\right)^{\alpha} A. \tag{21}$$

For this model,

$$Z_{Re,max} = \frac{R}{2}, \tag{22}$$

$$Z_{Im,max} = -\frac{R\sin(\alpha\pi/2)}{2(1+\cos(\alpha\pi/2))}, \tag{23}$$

$$\omega_{max} = \left(\frac{R\kappa A}{\ell}\right)^{-(1/\alpha)}\left(\frac{C_{dl}\ell}{\kappa}\right)^{-1}. \tag{24}$$

5.2. Model II

$$Z = \frac{1}{Y_A + Y_B}, \tag{17}$$

where

$$Y_A = \frac{\kappa}{\ell}\left(\frac{j\omega C_{dl}A\ell}{\kappa}\right)^{\alpha_A} A_A \tag{18}$$

and

$$Y_B = \frac{\kappa}{\ell}\left(\frac{\ell}{\kappa R_{ct}} + \frac{j\omega C_{dl,B}\ell}{\kappa}\right)^{\alpha_B} A_B. \quad (19)$$

For this model, the author has not been able to obtain analytic results for the Nyquist maximum. However, the other three properties listed in Table 1 will be useful as discussed in the concluding section.

5.3. Model III

$$Z = \frac{1}{Y}, \quad (25)$$

where

$$Y = \frac{\kappa}{\ell}\left(\frac{\ell}{\kappa R_{ct}} + \frac{j\omega C_{dl}\ell}{\kappa}\right)^{\chi} A. \quad (26)$$

For this model,

$$Z_{Re,max} = \frac{1}{\lambda}\left[\cos\left(\frac{\pi}{2(1+\alpha)}\right)\right]^{\chi}\cos\left(\frac{\alpha\pi}{2(1+\alpha)}\right), \quad (27)$$

$$Z_{Im,max} = -\frac{1}{\lambda}\left[\cos\left(\frac{\pi}{2(1+\alpha)}\right)\right]^{\chi}\sin\left(\frac{\alpha\pi}{2(1+\alpha)}\right), \quad (28)$$

$$\omega_{max} = \frac{1}{R_{ct}C_{dl}}\tan\left(\frac{\pi}{2(1+\alpha)}\right), \quad (29)$$

where

$$\lambda = \frac{\kappa}{\ell}\left(\frac{\ell}{\kappa R_{ct}}\right)^{\chi} A. \quad (30)$$

6. Discussions, summary and conclusions

Model I is often used to fit depressed arcs in the Nyquist plots which are not semi-circular. We have shown in this paper that this model is fundamentally flawed. A model was advanced for these depressed arcs and there is a clear case that one takes a fresh look at systems exhibiting these arcs using the diagnostic tests developed here. Table 1, for example, can be used to distinguish between model I and model II. While the high and low frequency slopes are equal for model I, the high frequency slope for model II is equal to or greater than the low frequency slope. Further, the intercept on the real axis is dependent on the electrolyte conductivity κ for model II; in fact, the logarithm of this intercept plotted versus $\log\kappa$ should be a straight line with slope $(\alpha_n - 1)$. On the other hand, this intercept is given by the empirical resistance R in model I; as model I does not have a physical/mathematical basis, R can at best be taken as a fitting parameter. Model III is very distinct from both model I and model II; its low frequency Nyquist slope is infinity and the high frequency slope is $\tan(\alpha\pi/2)$. The intercept on the real axis, for model III,

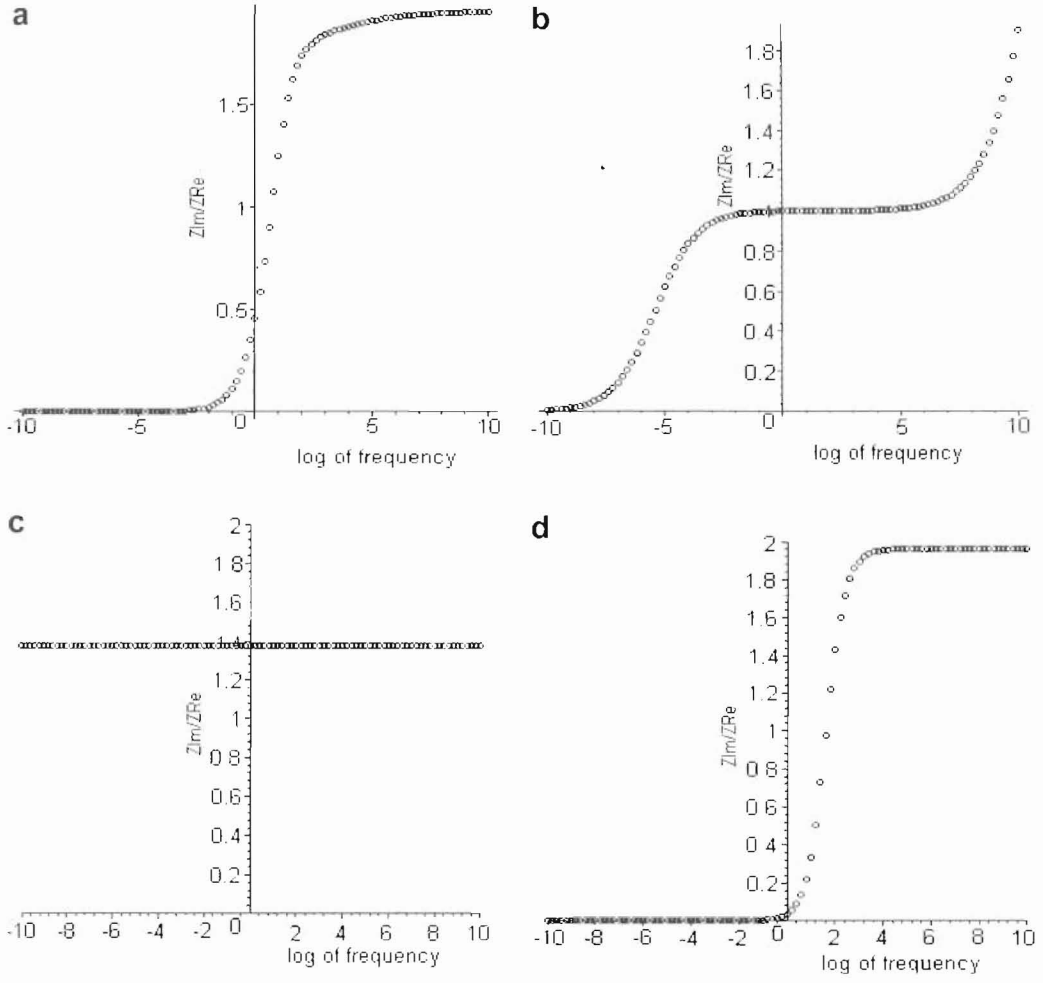

Fig. 4. Bode phase plots for model II. (a) $\alpha_A = 0.7$, $\alpha_B = 0.5$, $f_A = 0.99$ and $f_B = 0.01$. (b) $\alpha_A = 0.5$, $\alpha_B = 0.9$, $f_A = 0.9$ and $f_B = 0.1$. (c) $\alpha_A = 0.6$, $\alpha_B = x$, $f_A = 1$ and $f_B = 0$. (d) $\alpha_A = x$, $\alpha_B = 0.7$, $f_A = 0$ and $f_B = 1$. Other parameters are as in Figs. 1 and 2. x is any value between 0.5 and 1.

depends on the electrolyte conductivity κ in a way similar to that for model II.

Instead of Nyquist plots, we can also use Bode phase plots to represent our new model. In Fig. 4, we have plotted the ratio

$$-\frac{Z_{Im}}{Z_{Re}}$$

against the logarithm of frequency. This ratio, as shown in Appendix A, approaches zero for small frequency, while its high frequency limit is

$\tan(\alpha_A\pi/2)$ for $\alpha_A > \alpha_B$

and

$\tan(\alpha_B\pi/2)$ for $\alpha_B > \alpha_A$.

For example, in Fig. 4a, a single wave is observed showing clearly the high frequency limit as 1.962 corresponding to $\alpha_A = 0.7$. In Fig. 4b, two waves are seen, the first one corresponding to $\alpha_A = 0.5$ and the second one corresponding to $\alpha_B = 0.9$. Fig. 4c is for the case where only the A-type region is present on the electrode surface, i.e. a pure CPE. Fig. 4d is for the case where only the B-type region is present showing the high frequency limit as 1.962 corresponding to $\alpha_B = 0.7$. Hence it appears that the Bode phase plots will be useful, in favorable parametric regimes, to identify the presence of the A and B type regions on the electrode.

Eqs. (22)–(24) and Eqs. (27)–(29) provide more diagnostic checks for model I and III respectively. For example, for model I, $(-Z_{Im,max}/Z_{Re,max})$ should be equal to $\sin(\alpha\pi/2)/(1+\cos(\alpha\pi/2))$ and $\log\omega_{max}$ plotted versus $\log\kappa$ should be a straight line with slope $(\alpha-1)/\alpha$. For model III, $(-Z_{Im,max}/Z_{Re,max})$ should be equal to $\tan\left(\frac{\alpha\pi}{2(1+\alpha)}\right)$ and ω_{max} is independent of κ and is inversely proportional to $R_{ct}C_{dl}$.

The depressed arcs are often reported in corrosion studies. For example, Polo et al. encountered it during the inhibition of corrosion on mild steel by tributylamine [11],Walter et al. invoked it for the impedance analysis of painted metals [6] and Marikkannu et al. found it for metals at various stages of phosphate coating [12]. In all such instances, the electrode surface consists of two regions, one permitting Faradaic reactions and the other prohibiting it. However the experimental data were not analyzed that way by these authors who used only model I. Hence we reiterate that numerical fit alone does not validate a model and that there is a clear case for reexamining the experimental data on depressed arcs using the diagnostics made available in the present work. It should also be worthwhile to carry out carefully designed experiments along the following lines: start with an electrode which exhibits a well defined purely capacitive CPE and introduce a suitable redox reaction after blocking parts of the electrode surface against Faradaic processes. Test the resulting Nyquist response using the diagnostics for model II. Further, if the electrode is not partly blocked, the diagnostic criteria for model III should apply.

Three closing remarks are in order: (i) all the analytic results presented in this paper for the Nyquist maxima and the Nyquist slopes for $\omega = 0$ and $\omega = \infty$ were confirmed by independent computer simulations of the ac response. (ii) These simulations further revealed that these limiting Nyquist slopes should be computed by carefully extrapolating the slope values from the finite frequency range used in the simulation. This remark applies to the analysis of experimental data as well. The limiting slopes obtained may be in error otherwise and (iii) We introduced a length scale ℓ in this paper. Clearly, any impedance or admittance should be independent of this ℓ. This is indeed so because the non-trivial area factors such as A_A also depend on ℓ and the combinations like $A_A \circ \ell^{\alpha-1}$ which alone enters the theory should be invariant.

Acknowledgements

Useful correspondences, before the start of the present work, with Professor Robert de Levie on depressed arcs and lemniscates are gratefully acknowledged.

Appendix A

In this appendix, we sketch the method of obtaining the slopes of the Nyquist curve at the limits $\omega \to 0$ and $\omega \to \infty$. The Nyquist slope at any point is given by:

$$\frac{dZ_{Im}}{dZ_{Re}} = \frac{Z'_{Im}}{Z'_{Re}}, \tag{A1}$$

where the primes denote differentiation with respect to the frequency ω or a quantity which depends on ω. As we started, in this paper, with expressions for the complex admittance Y, we first make the following connections.

$$Z = \frac{1}{Y}, \tag{A2}$$

$$Z_{Re} = \frac{Y_{Re}}{(Y_{Re}^2 + Y_{Im}^2)}, \tag{A3}$$

$$Z_{Im} = -\frac{Y_{Im}}{(Y_{Re}^2 + Y_{Im}^2)}. \tag{A4}$$

We then differentiate Z_{Re} and Z_{Im} with respect to the frequency (in practice, it is found convenient to define $\theta = \tan^{-1}(\omega C_{dl}R_{ct})$ and differentiate with respect to θ instead).

After some algebra, we obtain

$$\frac{Z'_{Im}}{Z'_{Re}} = \frac{Q + \frac{2}{P-(1/P)}}{1 - \frac{2Q}{P-(1/P)}}, \tag{A5}$$

where

$$P = \frac{Y_{Im}}{Y_{Re}} \tag{A6}$$

and

$$Q = \frac{Y'_{Im}}{Y'_{Re}}. \tag{A7}$$

Thus, the Nyquist slope has been related to the slope of the corresponding admittance curve and (Y_{Im}/Y_{Re}). Note that this result is general and independent of any model. Applying it to our model II, we obtain

$\omega \to 0$ case:

$P \to 0$

and

$Q \to \tan(\alpha_A\pi/2)$.

Using this in Eq. (A5),

$$\frac{Z'_{Im}}{Z'_{Re}} \to \tan(\alpha_A\pi/2).$$

$\omega \to \infty$ case:

case (i) $\alpha_A > \alpha_B$

$P \to \tan(\alpha_A\pi/2)$,

$Q \to \tan(\alpha_A\pi/2)$.

Using this in Eq. (A5),

$$\frac{Z'_{\mathrm{Im}}}{Z'_{\mathrm{Re}}} \to -\tan(\alpha_A \pi/2)$$

case (ii) $\alpha_B > \alpha_A$

$$P \to \tan(\alpha_B \pi/2),$$
$$Q \to \tan(\alpha_B \pi/2)$$

and

$$\frac{Z'_{\mathrm{Im}}}{Z'_{\mathrm{Re}}} \to -\tan(\alpha_B \pi/2).$$

Appendix B

In this appendix we derive results for the maximum point of the Nyquist curve.

B.1. Model I

$$Z = \frac{1}{\frac{1}{R} + Y} \tag{B1}$$

where

$$Y = \frac{\kappa}{\ell}\left(\frac{\mathrm{j}\omega C_{\mathrm{dl}}\ell}{\kappa}\right)^{\alpha} A, \tag{B2}$$

$$= \lambda(\omega)\mathrm{j}^{\alpha} \tag{B3}$$

with

$$\lambda(\omega) = \frac{\kappa}{\ell}\left(\frac{\omega C_{\mathrm{dl}}\ell}{\kappa}\right)^{\alpha} A.$$

$$\therefore \quad Z = \frac{1}{\frac{1}{R} + \lambda(\omega)\cos(\alpha\pi/2) + \mathrm{j}\lambda(\omega)\sin(\alpha\pi/2)}. \tag{B4}$$

We now differentiate with respect to λ instead of ω and take the ratio of the λ-derivatives:

$$\frac{Z'_{\mathrm{Im}}}{Z'_{\mathrm{Re}}} = \frac{\sin(\alpha\pi/2)\left(\frac{1}{R^2} - \lambda^2\right)}{\cos(\alpha\pi/2)\left(\frac{1}{R^2} + \lambda^2\right) + \frac{2\lambda}{R}}. \tag{B5}$$

Clearly, the Nyquist maximum occurs when

$$\lambda = \frac{1}{R}.$$

$$\therefore \frac{\kappa}{\ell}\left(\frac{\omega_{\max} C_{\mathrm{dl}}\ell}{\kappa}\right)^{\alpha} A = \frac{1}{R} \tag{B6}$$

and

$$\omega_{\max} = \left(\frac{\kappa}{C_{\mathrm{dl}}\ell}\right)\left(\frac{\ell}{\kappa R A}\right)^{1/\alpha}. \tag{B7}$$

Using

$$\lambda = 1/R$$

in the expressions for

$$Z_{\mathrm{Re}} \quad \text{and} \quad Z_{\mathrm{Im}}$$

we obtain

$$Z_{\mathrm{Re,max}} = \frac{R}{2}, \tag{B8}$$

$$-Z_{\mathrm{Im,max}} = \frac{R\sin(\alpha\pi/2)}{2(1+\cos(\alpha\pi/2))}. \tag{B9}$$

B.2. Model III

Eq. (26) may be conveniently rewritten as

$$Y = \lambda \frac{\exp(\mathrm{j}\alpha\theta)}{(\cos\theta)^{\alpha}}, \tag{B10}$$

where

$$\theta = \tan^{-1}(\omega C_{\mathrm{dl}} R_{\mathrm{ct}}) \tag{B11}$$

and

$$\lambda = \frac{\kappa}{\ell}\left(\frac{\ell}{\kappa R_{\mathrm{ct}}}\right)^{\alpha} A. \tag{B12}$$

From this it is quite straightforward to find the impedance Z and its real and imaginary parts Z_{Re} and Z_{Im}. Take now the ratio of the derivatives with respect to θ and simplify to obtain

$$\frac{Z'_{\mathrm{Im}}}{Z'_{\mathrm{Re}}} = -\frac{1}{\tan((1+\alpha)\theta)}. \tag{B13}$$

Equating this to zero, we locate the maximum as

$$(1+\alpha)\theta_{\max} = \pi/2 \tag{B14}$$

and

$$\omega_{\max} = \frac{1}{C_{\mathrm{dl}} R_{\mathrm{ct}}} \tan\left(\frac{\pi}{2(1+\alpha)}\right). \tag{B15}$$

Substituting the value of $\theta_{\max}$ in Z_{Re} and Z_{Im}, $Z_{\mathrm{Re,max}}$ and $Z_{\mathrm{Im,max}}$ follows.

References

[1] Bosco Emmanuel, J. Electroanal. Chem. 605 (2007) 89–97.
[2] Bosco Emmanuel, Eng. Anal. Bound. Elem. 32 (2008) 770–777.
[3] R. de Levie, in: P. Delahay (Ed.), Advances in Electrochemistry and Electrochemical Engineering, vol. 6, Wiley, New York, 1967.
[4] E. Barsoukov, J.R. Macdonald, Impedance Spectroscopy (Theory, Experiment and Applications), 2nd ed., Wiley Interscience, New Jersey, 2005.
[5] D.D. Macdonald, Electrochim. Acta 51 (2006) 1376–1388.
[6] G.W. Walter, D.N. Nguyen, M.A.D. Madura Singhe, Electrochim. Acta 37 (1992) 245–262.
[7] M.E. Orazem, P. Shukla, M.A. Membrino, Electrochim. Acta 47 (2002) 20–27.
[8] R. de Levie, J. Electroanal. Chem. 281 (1990) 1–21.
[9] P. Los, A. Lasia, H. Menard, L. Brossard, J. Electroanal. Chem. 360 (1993) 101.
[10] A. Hasbach, U. Retter, K. Siegler, W. Kautek, J. Electroanal. Chem. 561 (2004) 29–35.
[11] L. Polo, E. Cano, J.M. Bastidas, Corros. Prevent. Contr. 51 (2004) 55–59.
[12] C. Marikkannu, K. Balakrishnan, Bull. Electrochem. 15 (1999) 156–159.